Eur. Phys. J. E (2018) **41**: 3
DOI 10.1140/epje/i2018-11614-y

THE EUROPEAN PHYSICAL JOURNAL E

Regular Article

Self-assembly of magnetically functionalized star-polymer nano-colloids

Ronald Blaak[a] and Christos N. Likos

Faculty of Physics, University of Vienna, Boltzmanngasse 5, A-1090 Vienna, Austria

Received 20 October 2017 and Received in final form 18 December 2017
Published online: 12 January 2018

Abstract. We explore the potential of star-polymers that carry super-paramagnetic nano-particles as end-groups with respect to the single-molecule self-assembly process. With the aid of molecular dynamics simulation, the configurations of these macromolecules are analyzed as a function of functionality, magnetic interaction strength, and the length of the polymeric arms. By means of an external magnetic field the nano-particles can be controlled to form static or dynamic dipolar chains, resulting in conformations of isolated stars that can be characterized by the average number of chains and length. The single-molecule conformation diagram in the plane of magnetic interaction strength *vs.* the star-functionality is obtained. Further, the molecules are characterized by means of various shape and size order parameters.

1 Introduction

This conformation dependence on solvent quality can be exploited by combining different monomeric units within a polymer. The simplest example of that is an AB-diblock copolymer, where only two different building units are being used. One segment of the polymer chain, A, consists for instance of a number of identical solvophobic monomers, while the other segment B is formed by a number of solvophilic monomers. Already this type of polymeric chains, that can be characterized by the relative fraction of both types of units and the polymer-solvent interaction parameter, result in a surprisingly complex state diagram where the polymers can form spherical micro-structures, hexagonally packed cylinders, lamellar and bicontinous phases [1]. An obvious extension is to consider ABA- or BAB-triblock copolymers, where we can, depending on the composition and concentration, find normal and flower-like micelles but also connected networks [2,3]. An even more extreme version of this is found in DNA origami, where tailored single-stranded base-sequences can be used to create long molecular chains that can self-assemble in a particular target structure, such as a cube, a box, and various other shapes [4–6].

An altogether different approach than variations in sequences to generate more complex types of behavior, is to synthesize branched structures. This can be in the form of uniform side-branches on a polymeric backbone, dendrimers, or star-polymers [7–11]. In the latter case, a number of polymeric chains are grafted on a mutual core or, for instance, connected by a central dendrimer and are characterized by the number and length of the polymeric arms. Similar to their linear counterparts, also for these star-polymers a compactification transition can be induced by manipulating external conditions such as solvent quality and temperature. Such behavioral changes can be enhanced by the inclusion of functional units within the polymer chains that for example can be ionized.

A simple, but nevertheless fascinating, example of functionalized macromolecules is found in telechelic star-polymers, where the arms are formed by AB-diblock copolymer [12,13]. In particular the case where the solvophilic segment is located in the center, and hence forcing the solvophobic chain-segment to extend in the solvent, results in some unexpected types of behavior. Not only do they display the ability to form gel networks and micelles, but depending on the ratio of A and B monomers and the functionality (number of arms) of the star-polymer, such micelles self-organize in larger worm-like structures [14,15]. Even more striking is the possibility to form a "soft-patchy particle" by individual isolated stars, for which the solvophobic polymer tails reversibly merge into one or several clusters that surround the solvophilic core. The number of these clusters is determined by the functionality and other details of the architecture [16–18]. These patchy-like particles, themselves can be employed to stabilize various crystalline lattices with coordination numbers compatible with the number of patches found in the single isolated polymer-stars [18,19].

Soft-patchy particles are the more recent extension of the anisotropic interaction potentials as were for instance used in primitive models for water [20] and silica [21].

[a] e-mail: ronald.blaak@univie.ac.at

These models on the atomic scale were in the 1990s extended to more mesoscopic particle sizes to model globular proteins [22] and to study self-assembly processes [23]. For and overview of patchy particles as well as their synthesis we refer the reader to refs. [24,25]. The common factor in these particles and models is the rigidity in their shape and the location of the patches or interaction sites. In the case of soft-patchy particles, their overall shape, the size and location of the patches, and even the number of patches need not be constant as the patches arise from a reversible self-assembly.

The behavior of functionalized star-polymers is for an important part determined by their architecture and can be controlled externally by concentration, temperature, and solvent quality [26]. Here we want, by means of computer simulations, to explore the potential of functionalized star-polymers for which the internal and mutual interactions can be influenced in a more direct fashion. This is possible by considering homogeneous star-polymers, where only the terminal groups are functionalized with magnetic nano-particles [27,28] and more particular super-paramagnetic particles. Consequently, the presence and strength of the magnetic interactions are directly controlled by the application of an external magnetic field that can be employed in both static and dynamic configurations. Similar to their telechelic counterparts, also here the end-groups can, depending on the interaction strength, form clusters. These aggregates, however, will be formed by magnetically induced dipolar chains rather than compact solvophobic patches. It should be stressed that, to the best of our knowledge and to date, such magnetically functionalized star-polymers have not been synthesized, but given the current state of synthesis techniques available this seems to be feasible.

Given the explorative nature of the present study, we start with formulating a simple semi-qualitative simulation model that captures the essence of the system in sect. 2. Individual model star-polymers for various functionality and interaction strength are simulated in order to map out a single-state conformation diagram in sect. 3. In sect. 4 we analyze these conformations by means of various size and shape parameters. Section 5 focuses on the characterization of the dipolar chains that are formed during the simulations and the density profiles of magnetic particles are displayed in sect. 6. We conclude with a discussion and summary of the main results, as well as an outlook, in sect. 7.

2 The model

Since we are interested in the exploration of the behavior and properties of magnetically functionalized star-polymers and the manner in which their conformation can be controlled by their magnetic end-groups that interact with each other due to the presence of an external field, we construct a generic model for such macromolecules that can easily be extended in complexity, but for reasons of convenience is stripped to its bare essentials. To this end we employ a bead-spring model, which is governed by the repulsive Week-Chandler-Andersen (WCA) [29] interaction between monomers and the finitely extensible nonlinear elastic potential (FENE) [30] to restrict distances and model molecular bonds.

Within our star-polymer we distinguish three different types of particles. In the center is the core (O) to which f polymer arms are attached. The arms are represented by a number N of identical monomeric beads (A) and terminate in a single super-paramagnetic particle (B). The direct interaction between any two of these beads has the form of a shifted and truncated Lennard-Jones or WCA potential complemented with a hard-core contribution and is purely repulsive in nature:

$$\Phi_{\mu\nu}^{(\mathrm{WCA})}(r) = \begin{cases} \infty, & \text{if } r - D_{\mu\nu} \leq 0, \\ 4\epsilon \left[\left(\dfrac{\sigma}{r - D_{\mu\nu}} \right)^{12} \right. & \\ \left. - \left(\dfrac{\sigma}{r - D_{\mu\nu}} \right)^{6} + \dfrac{1}{4} \right], & \text{if } 0 < r - D_{\mu\nu} < 2^{1/6}\sigma, \\ 0, & \text{if } r - D_{\mu\nu} \geq 2^{1/6}\sigma. \end{cases} \tag{1}$$

Here the subscripts μ and ν are labels for the type of units we consider, ϵ characterizes the strength of the interactions, σ is the diameter of the monomers that constitute the polymer arms and determines the interaction range, and the $D_{\mu\nu}$ are the hard-core size of the respective beads. Note that we already have introduced the first simplification by choosing the interaction strength $\epsilon = k_B T$ and range σ, which are our chosen units of energy and length, respectively, to be the same for all species.

For the monomers of type A that form the polymer arms we assume that there is no hard core present, *i.e.*, $D_{\mathrm{AA}} = 0$, which is compatible with many bead-spring models of a similar nature. For the central core of the star-polymer we assume to have a hard core that we fix by $D_{\mathrm{OO}} = 2\sigma$. Although strictly speaking, unless the polymers arms would be grafted on some colloidal particle, such a hard core is absent in real star-polymers where the center would be formed by a dendrimeric type of molecule. The concentration of monomers of different arms near the center of the star, however, make it effectively an excluded region. Given the goal of the present study, the microscopic details of the modeling of the center of the functionalized star-polymer is not particular relevant as its main role is to graft these different arms together. In addition to this physical motivation it serves from a computational aspect as a way to limit excessively high energies and forces in this location and to avoid potential computational problems. Finally, we choose $D_{\mathrm{BB}} = \sigma$ to represent the fact that a nano-particle that forms the end-group of the polymer arm has an impenetrable core made of some magnetic material. The various cross-interactions are obtained by taking the mean averages of the corresponding monomer sizes, *i.e.*, $D_{\mu\nu} = (D_{\mu\mu} + D_{\nu\nu})/2$.

To maintain the architecture intact, we model the bonds between successive units of type μ and ν along an

arm via the FENE potential [30]

$$\Phi_{\mu\nu}^{(\mathrm{FENE})}(r) = -\frac{k\Delta^2}{2}\ln\left[1-\left(\frac{r-D_{\mu\nu}}{\Delta}\right)^2\right]. \qquad (2)$$

Also here we measure the distance for the bonds with respect to the relevant hard-core diameter. The strength of the spring constant is chosen to be $k = 15\epsilon/\sigma^2$ and the maximal bond length is restricted to $\Delta = 1.5\sigma$. These values correspond to a situation where bonds will not cross, which for the present study —where we focus on static properties— is not truly relevant, but becomes important in future studies on the dynamics. Similar to the WCA interaction, we have adopted a simplification in parameter space by choosing the values of both parameters k and Δ to be independent of the bead species. Also note that by this choice of bonds, a polymer arm is not grafted on the core at fixed position, but is attached by means of a mobile site on the surface of a sphere; its movement is restricted only by mutual steric interactions with other arms.

The final ingredient that is required for the model are the magnetic interactions that affect the end-groups only. As a first approximation the mutual interaction between two magnetic beads is modeled by a dipole-dipole contribution

$$\Phi^{(\mathrm{mag})}(\vec{r}) = \frac{\mu_0}{4\pi r^3}\left[\vec{m}_1\cdot\vec{m}_2 - 3(\vec{m}_1\cdot\hat{r})(\vec{m}_2\cdot\hat{r})\right]; \qquad (3)$$

here $\vec{m}_1$ and $\vec{m}_2$ are the magnetic dipole moments of both nano-particles and μ_0 the magnetic constant in vacuum separated by a vector $\mathbf{r}$ (with $\hat{r} = \mathbf{r}/|\mathbf{r}|$). As we consider super-paramagnetic particles here, the dipole moments are induced by an externally applied homogeneous magnetic field. It will be assumed that the magnitude $m = |\mathbf{m}|$ of these dipole moments is the same for every magnetic bead and is at all times perfectly aligned with the external field chosen along the z-direction of the reference system. This implies that we neglect local effects that cause variations in dipole strengths and directions for the nano-particles that approach each other. Consequently, the magnetic interaction simplifies to

$$\Phi^{(\mathrm{mag})}(\vec{r}) = \frac{\mu_0 m^2}{4\pi r^3}\left[1-3(\hat{r}\cdot\hat{z})^2\right]. \qquad (4)$$

We also introduce the dimensionless parameter $\lambda \equiv \mu_0 m^2/(4\pi\sigma^3\epsilon)$ to characterize the relative strength of the magnetic interaction, which corresponds to the energy of two aligned magnetic beads in the side-by-side configuration at a distance σ. Within this model, such a close approach is actually not possible by virtue of the soft shell that is assumed to surround the magnetic core and which ensures that the effective minimum distance is almost twice as large as the core diameter. It should also be pointed out that, similar to the mobility of the monomers that bind the arms to the core of the star, also the magnetic beads are bound without restriction to the end of the arms, *i.e.*, the direction of the magnetic dipoles within the simulation can rotate in an unhindered manner with respect to the backbone of the polymer arm. Note that in the case of magnetic beads with a permanent dipole moment their directions would be fixed with respect to the terminal monomers of the polymer arms. Since we assumed to have induced dipoles this is not the case here.

The magnetic particles we consider here would be typically 20 nm in diameter and consisting of a coated super-paramagnetic core of 10 nm made of for instance ferumoxide [27]. In the strong field limit of 10 kG this would results in a value of $\lambda \approx 100$. This value decreases with a weaker field strength, a smaller core size, a thicker coating layer, and a stronger repulsive interaction between coating and polymer. For these small sizes the core forms essentially a single domain, hence the validity of a macro-spin treatment. Strictly speaking, the model is also applicable to paramagnetic materials provided the response to the external field is strong enough, because the external field strength only appears implicitly within the magnitude of the dipole moment m and the interaction strength λ. In an experimental setup, however, this would result in undesirable hysteresis effects on changing the field strength.

3 The single-star conformation diagram

For computational reasons the functionality f (number of arms) of the star-polymers is restricted to the range 5–50 and the number of monomers per arm N are 30, 40, and 50. We will limit ourselves here, however, to presenting only results for the case of $N = 50$ monomers per polymer arm, because the behavior for both shorter arms is qualitatively the same. Simulations were performed on single star-polymers using the ESPResSo package [31] with a Langevin thermostat and fixed center of mass. Since our goal is to describe the static properties of these systems, we choose the masses of all types of monomers to be the same. Strictly speaking, the core and the magnetic beads should be heavier, but our choice facilitates the mobility specially of the latter units and should not affect the physical properties of interest.

Initial configurations were chosen randomly from independent equilibrated trajectories of stars without magnetic interactions. All properties have been obtained from averaging over 16 different and independent realizations. In fig. 1 a few typical snapshots from the simulations of these isolated stars are displayed for different functionality f and relative magnetic interaction strength λ.

Because of the perfect alignment of the magnetic dipole moments with the imposed external field, the description of their interaction is a rather simple one, *i.e.*, there is an attraction for head-to-tail arrangements that is limited by the short-range repulsion originating from the WCA interaction, and a repulsion for the side-by-side arrangements. Consequently, from an energetic point of view the magnetic beads can only aggregate into chains or remain separated. The formation of chains, however, is opposed by the steric interaction of the polymer arms, the loss of entropy by a restricted direction of the arm, and the limitation caused by the finite length of the polymer arms.

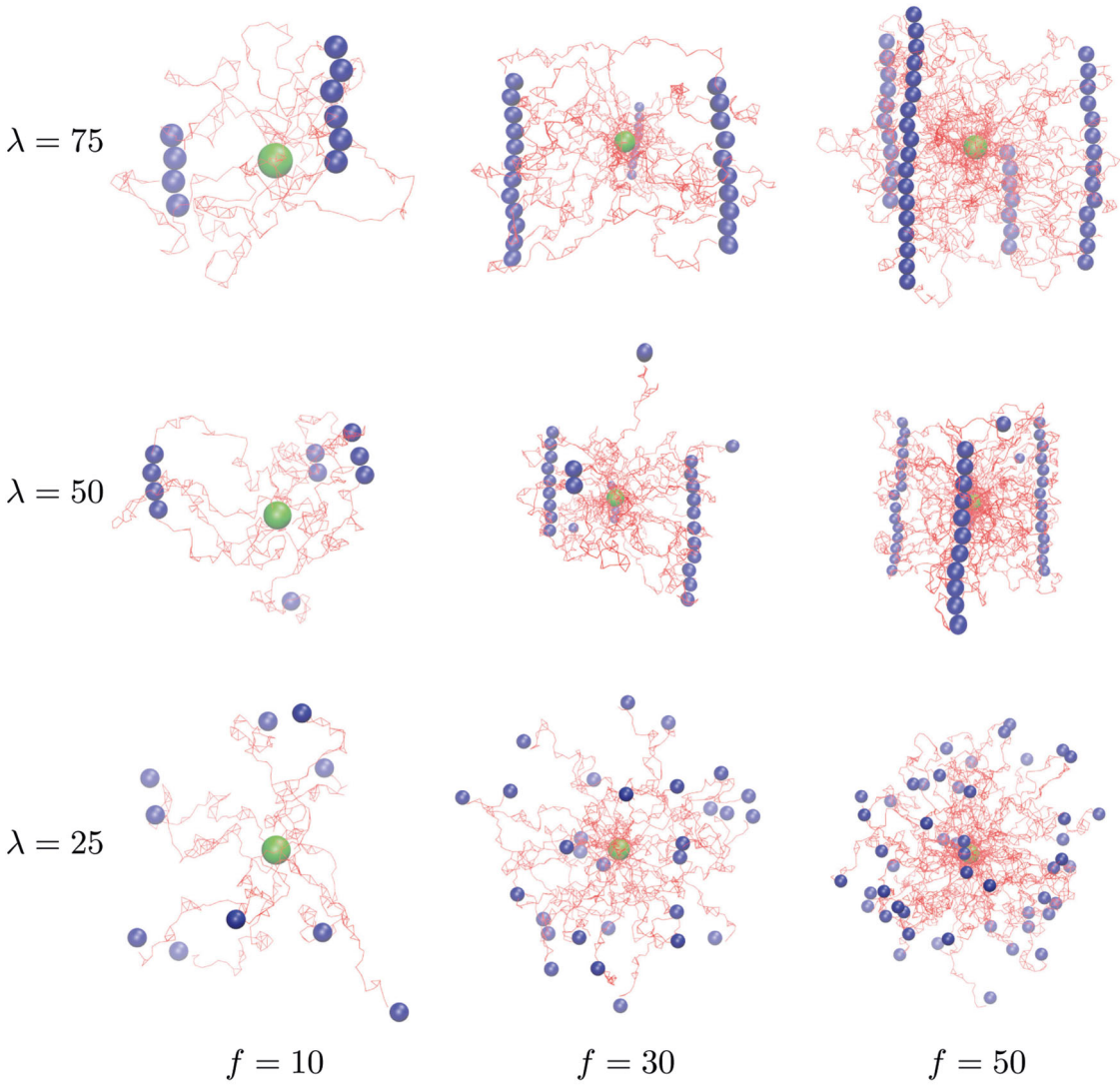

Fig. 1. Typical snapshots of isolated magnetically functionalized star-polymers in an external field along the vertical direction. The green and blue spheres are the core and magnetic beads, respectively. For clarity, the monomers that constitute the polymer arms are omitted in this presentation and only the backbone is indicated in red. From left to right the functionality $f = 10$, 30, and 50. The relative magnetic strength from top to bottom $\lambda = 75$, 50, and 25.

For weak magnetic interactions we end up with normal star-polymers, where terminal end-groups briefly interact but are not able to support the formation of stable aggregates. For the lowest interaction strength $\lambda = 25$, the behavior and all considered properties are fully consistent with non-functionalized star-polymers [32]. On increasing the external field, the energetic gain due to the formation of small chains will begin to outweigh the entropic losses. The averaged number of these chains will obviously depend on the particular functionality of the star-polymer as well as on the strength of the external magnetic field. On increasing the magnetic interaction even more, the secondary energetic cost arising from open ended chains becomes more important than the entropic loss of stretching arms, resulting in longer chains and a decrease of their number.

This aggregation of end-groups in magnetically functionalized star-polymers is qualitatively similar to that of the self-assembly of telechelic stars, for instance by Capone *et al.* [18,19]. In those investigations the arms of the star-polymers are diblock copolymers that consist of solvophilic heads attached to the core and solvophobic tails. The corresponding driving force for clustering and the consequential formation of a type of patchy particle, is imposed by the minimization of the surface of the solvophobic aggregates exposed to the solvent. Such aggregates by default are therefore more spherical and compact in nature than the dipolar chains formed here.

To map out the generic behavior of the self-assembled structures, simulations were performed for functionalities $f = 5, 10, \ldots, 50$ and interaction strengths $\lambda = 25$–100. In these simulations we determine the number and length

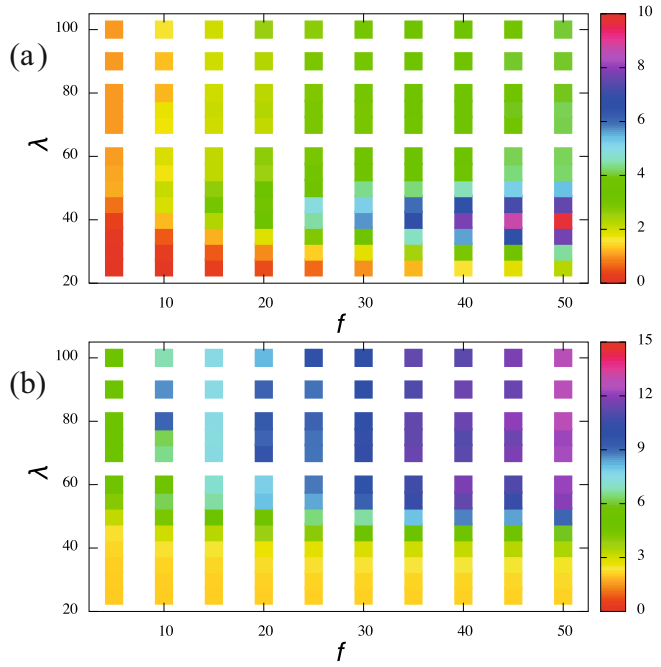

Fig. 2. Single-star configuration diagram of (a) the average number of chains to be found and (b) the average number of particles per chain (≥ 2) as functions of the functionality f and relative interaction strength λ for magnetically functionalized star polymers with $N = 50$ monomers per polymer arm.

of dipolar chains; for the formation of a chain at least two particles have to bind. We consider magnetic particles to be part of the same chain whenever their distance is less than 2.5σ and their relative positions are such that the magnetic interaction is attractive. Since the magnetic bonds in the chains are reversible, the length of individual chains as well as their number fluctuate and we observe merging and breaking of chains within the duration of the simulations. Only for very high interaction strengths this is no longer the case and nearly irreversible bonds are formed.

The resulting averages for the number and lengths of chains for the $N = 50$ case are shown in fig. 2. Within this analysis we have discarded single, isolated beads from both averages. Even for the lowest interaction strength $\lambda = 25$ considered here we observe small chains. The probability for an arm to contribute to a chain grows from approximately 0.01 for functionality $f = 5$ to about 0.1 for $f = 50$. Here, the higher functionality enhances the chance for encounters between end-groups by restricting their freedom due to the neighboring polymer arms. Although longer chains for such weak interactions strengths are observed, the average length remains only slightly larger than two units.

On increasing the magnetic interaction strength ($\lambda \approx$ 30–50), the average number of chains that is being formed grows steadily, as does their average length. This trend continues, until the interaction becomes strong enough that the waiting time required for a chain to break up or an arm to detach from the end of a chain becomes of the

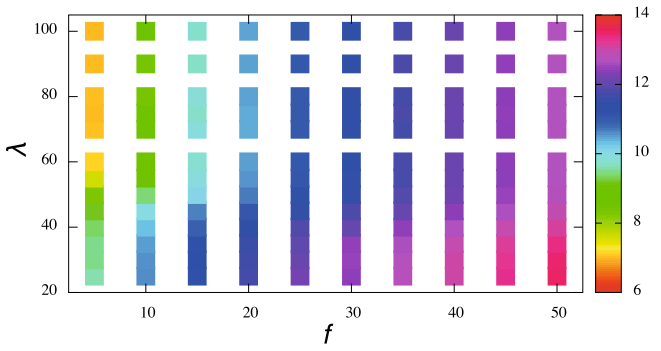

Fig. 3. The radius of gyration R_g/σ of a single magnetically functionalized star-polymer as a function of the functionality f and interaction strength λ.

same order of magnitude as the time needed for chains or arms to find each other and merge. Beyond that intermediate range of interaction strengths ($\lambda \gtrsim 50$), the average length still increases, but the number of chains by necessity of the conservation of the number of magnetic beads has to decrease. This latter effect is the origin of the maximum in the average number of chains that can be seen in fig. 2(a) for the range $\lambda \approx$ 30–50 and $f \approx$ 40–50.

The main consequence arising from having shorter polymer arms (the cases $N = 30$ and 40 that are not shown here) is the higher penalty on the longer dipolar chains due to the stretching of polymer arms that connect to the outer ends. This implies that there are on average a bit more and at the same time smaller chains found in the star. However, the picture that emerges for these cases is qualitatively the same.

It should also be pointed out that for the highest interaction strengths and lowest functionalities some minor discrepancies with respect to a smooth behavior are visible in fig. 2, in particular for the case $f = 10$, where the average number of clusters and their average length obtained from the simulations as function of the increasing interaction strength shows some non-monotonic behavior. Here, in some of the different simulations already the more stable single chain of length 10 were formed, whereas others did not yet do so. The process of breaking, diffusion, and merging of chains for these high interaction strengths is however very slow. To some extent this is also due to the way the magnetic interaction was imposed, *i.e.*, via a quench from an equilibrated star-polymer without external magnetic field. These uncertainties could easily be removed by simulations an order of magnitude longer, a slower incremental increase of the magnetic interaction via the external field, or using the technique of parallel tempering or replica exchange; however, this would not significantly affect the main results.

4 Size and shape

In order to examine the shape and form of the functionalized star-polymers, we have measured the radius of gyration and the other shape parameters that can be obtained

from the gyration tensor $S_{\alpha\beta}$ [33]. The latter is an object that can be easily obtained from simulations, as it only requires the input of the coordinates $\mathbf{r}^i$ of all $\mathcal{N}$ particles of a molecule and their corresponding center of mass $\mathbf{r}^0$

$$S_{\alpha\beta} = \frac{1}{\mathcal{N}} \sum_{i=1}^{\mathcal{N}} \left(r_\alpha^i - r_\alpha^0\right) \left(r_\beta^j - r_\beta^0\right), \quad \alpha, \beta = 1, 2, 3. \quad (5)$$

The radius of gyration R_g, which is a measure for the effective size of a molecule, can be obtained from the trace of the gyration tensor, *i.e.*, $R_g^2 = \mathrm{Tr}(S_{\alpha\beta})$. As is to be expected, the size of a star-polymer increases with increasing functionality as can be seen in fig. 3 where the results for the radius of gyration are shown. This trend is merely due to the fact that an increased functionality results in a higher effective density in the core region of a star and the locally increased steric interactions expel the arms more to the outer regions. In a similar fashion, also the increased magnetic interaction affects the size of a star. In this case, however, it is the increase in the number of functionalized monomers that participate in the dipolar chain formation that anchor the polymeric arms in a second point with limited distance to the center. This enforces a shorter core-to-end distance of the arms and results in an effectively reduced size of the whole star, which is an effect similar to what is found for telechelic star-polymers.

The characterization of the polymer-stars by means of the radius gyration is very limited, because it approximates the full object as a spherical one. Given the self-assembly of chains that takes place within the star on increasing the magnetic interaction strength, however, these stars are inherently asymmetric in nature. In lowest order those aspherical shape features can be captured by three different shape parameters that can be obtained from the gyration tensor eq. (5). They rely on the fact that the tensor by default is symmetric and therefore can be diagonalized to the form $\Lambda = [\lambda_1^2, \lambda_2^2, \lambda_3^2]$, where, the in general different principal moments, are ordered by requiring $\lambda_1^2 \geq \lambda_2^2 \geq \lambda_3^2$. The square root of these values correspond roughly with the dimensions of the molecule when it is approximated by an ellipsoidal shape and the corresponding eigenvectors with its orientation in space. From the eigenvalues we can also directly compute the asphericity b, the acylindricity c, and the anisotropy κ^2 defined as

$$R_g^2 = \lambda_1^2 + \lambda_2^2 + \lambda_3^2, \quad (6a)$$

$$b = \lambda_1^2 - \frac{1}{2}\left(\lambda_2^2 + \lambda_3^2\right), \quad (6b)$$

$$c = \lambda_2^2 - \lambda_3^2, \quad (6c)$$

$$\kappa^2 = \frac{b^2 + (3/4)c^2}{R_g^4}. \quad (6d)$$

By comparing the values of these related quantities we can determine whether a particular configuration of interest is more spherical ($b = c = 0$), prolate or oblate, and whether it possesses an axial symmetry or not.

The results for these shape parameters can be found in fig. 4. By comparing the different panels we observe

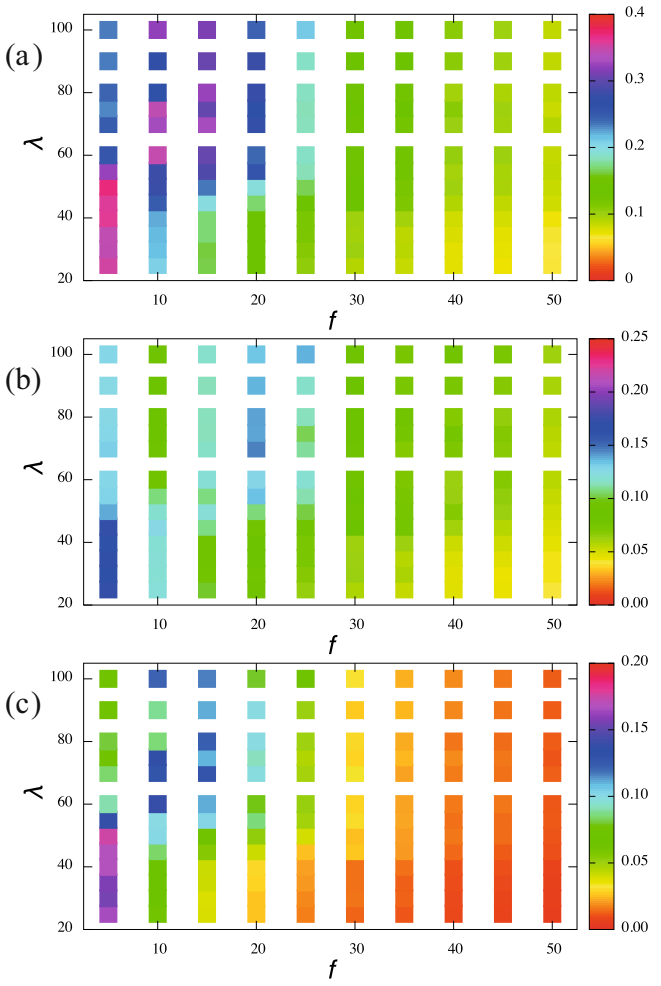

Fig. 4. The normalized (a) asphericity b/R_g^2, (b) acylindricity c/R_g^2, and (c) anisotropy κ^2 of a single magnetically functionalized star-polymer as a function of the functionality f and interaction strength λ.

from the small order parameter values that on the whole the star-polymers get more spherical for increasing functionality and for decreasing magnetic interaction strength, which is consistent with the observations above. Only for the lowest functionality, this appears not to be the case and we see an opposite trend, *i.e.*, the asphericity, the acylindricity and the anisotropy diminish but now for increasing interaction strength. Their values, however, do not go converge to zero but remain finite, which indicates that there is no proper spherical symmetry present. For these cases of low functionality and high interaction strength the underlying idea of a fairly homogeneous distribution of monomers breaks down. The reason is of course that in most of these cases a single dipolar chain is formed, which results in a very asymmetric type of object, where the center of mass is not close to the core particle of the star. It is a structure similar to what was labeled a "watermelon" configuration for telechelic star-polymers [16,17]. This behavior propagates to functionality 10 and 15, although here the number of chains tends to be two, a double watermelon structure, where the chains

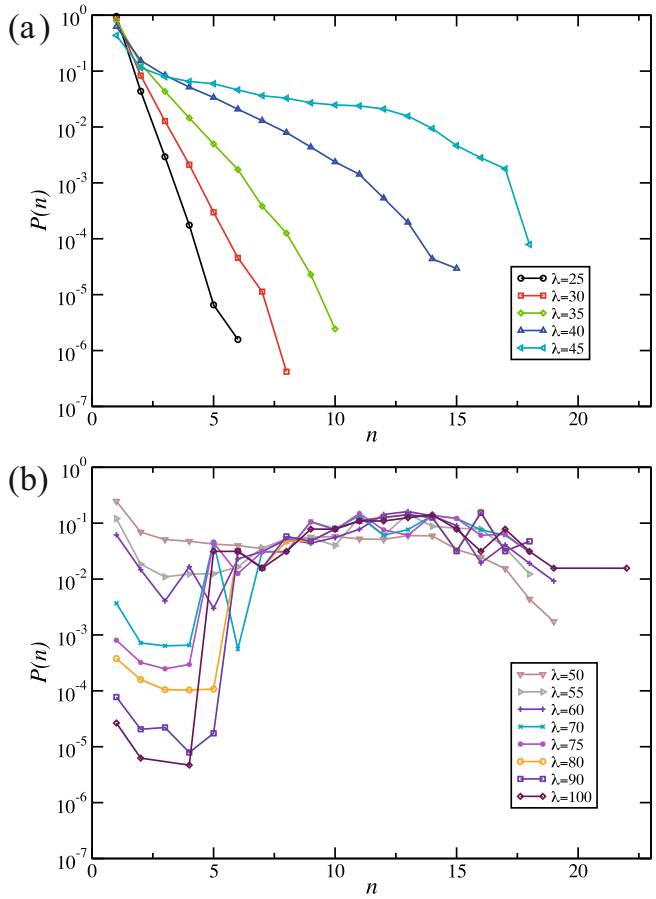

Fig. 5. The probability $P(n)$ for a chain to contain n dipoles for the interaction strengths λ (as labeled) and star-functionality $f = 50$. (a) Weak interactions ($\lambda \lesssim 50$) with an exponential decaying distribution and (b) strong interactions ($\lambda \gtrsim 50$) with a preferred chain length.

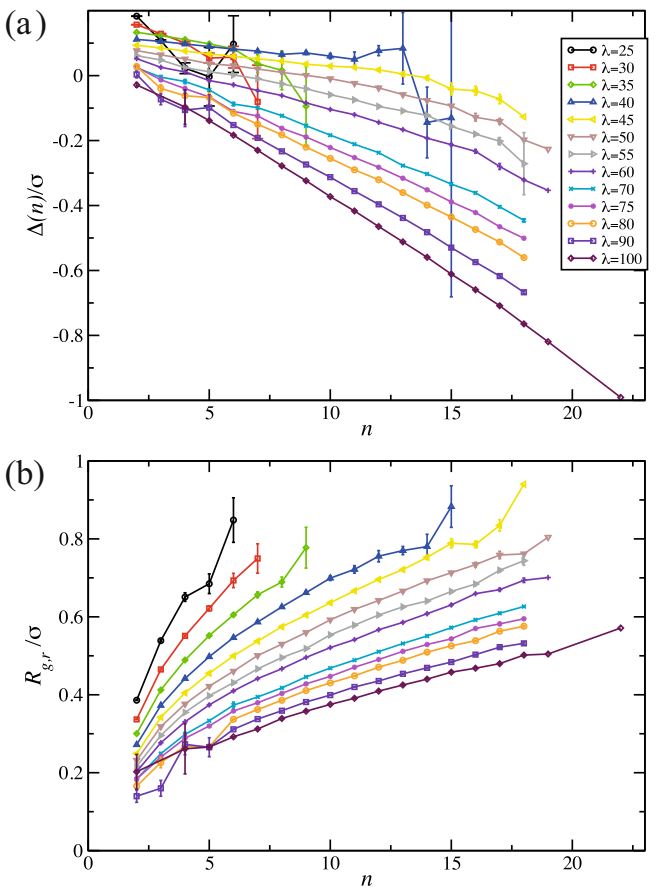

Fig. 6. (a) The deviation $\Delta(n)$ from the ideal end-to-end chain length (see eq. (7)) and (b) width of the chain $R_{g,r}$ as function of the number of particles n in the chains for star-polymers of functionality $f = 50$ at different interactions strengths λ.

are not necessarily opposite to each other with respect to the center of the star.

5 Chain properties

The length of chains that are formed for a given functionality and interaction strength fluctuates. Especially for low magnetic interaction strengths they can easily break and merge. Although we have shown the average chain lengths in fig. 2, we need to address the deviations from such average values. To this end, we measured the probability $P(n)$ that a chain has a particular length n, where we consider isolated magnetic beads to be a chain of length unity. The results from this calculation for the highest functionality $f = 50$ are presented in fig. 5 for the different interaction strengths.

There are essentially two domains and types of behavior. If the magnetic interactions are weak, clusters can easily break and merge and the length-distributions for $\lambda \lesssim 40$ are exponentially decaying with the chain length. This observation is consistent with the picture of a random aggregation process with a fixed energy gain per added unit, where in this case the step in energy is a combination of magnetic gain and entropic loss. On increasing the magnetic strength λ, the magnitude of this gain increases and longer chains can be formed, but shorter chains remain more likely to be found. For $\lambda \gtrsim 50$ we find that this is no longer the case and that it appears to actually be an optimal chain size. With the expected number of four chains for these stars (see fig. 2), this optimum value is 12–13 units. The distribution is, however, rather wide which explains the noisy shape of the curves due to limited sampling for the strongest interactions.

Due to the magnetic interaction of the perfectly aligned dipoles, the dipolar chains are in general quite straight. The end-to-end distance $d(n)$ of chains of length n is only weakly dependent on the strength of the interaction and is approximately $2(n-1)\sigma$. We denote deviations from this simple esitmated behavior by $\Delta(n)$

$$\Delta(n) = d(n) - 2(n-1)\sigma; \tag{7}$$

this quantity is depicted in fig. 6(a). $\Delta(n)$ shows a nearly constant growth for each of the interaction strengths. The actual average distance between two magnetic beads depends on the relative strength of the magnetic dipole-dipole attraction and the soft WCA-repulsion, and will

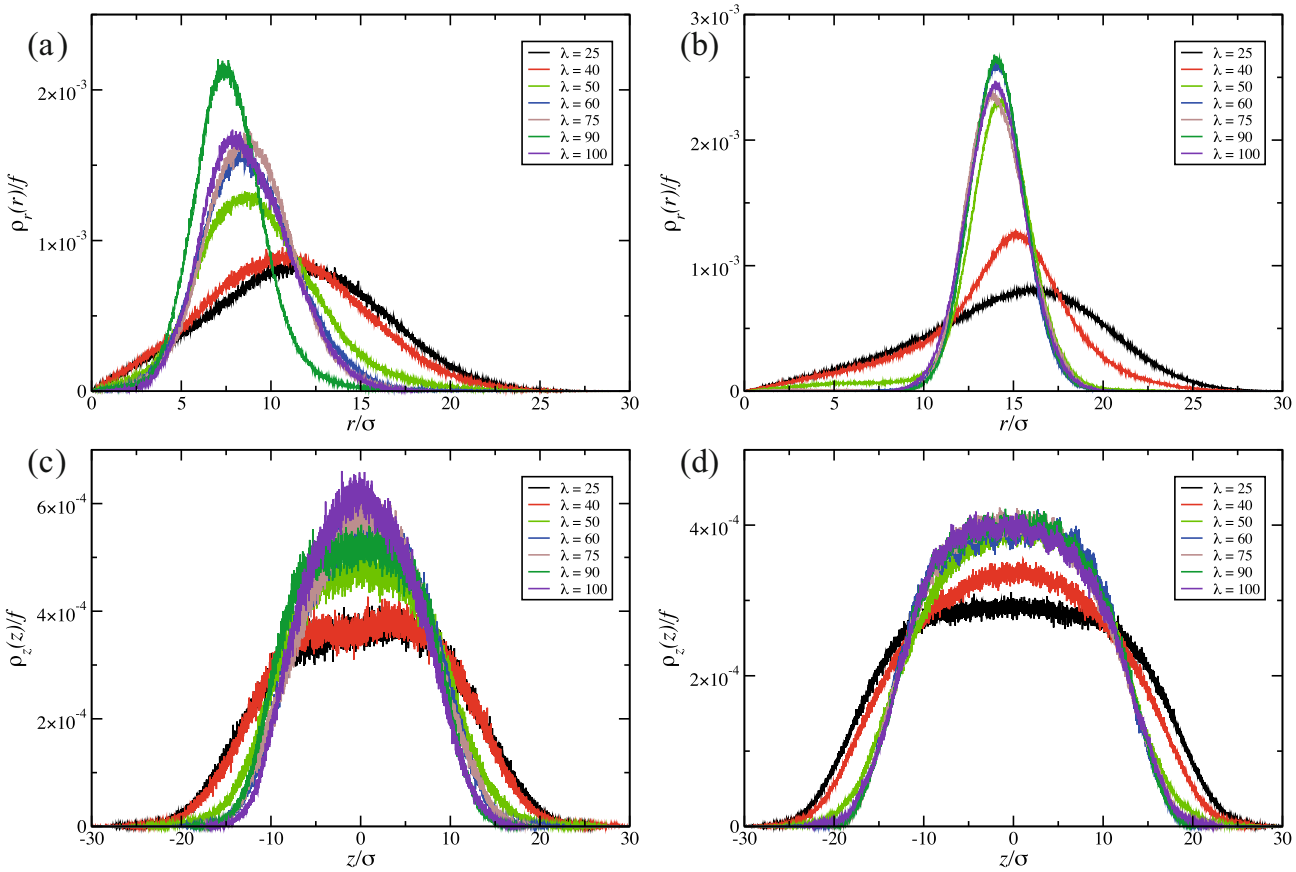

Fig. 7. The density profiles (a), (b) $\rho_r(r)/f$ and (c), (d) $\rho_z(z)/f$ of magnetic particles with respect to the center of mass of the star-polymer, for functionality (a), (c) $f = 10$ and (b), (d) $f = 50$ and for various interaction strengths λ (as labeled).

be slightly higher than 2σ for weak interactions and gets smaller for larger values of λ. It also shows a slight concave behavior. This corresponds to the fact that also beads that are further apart experience the magnetic attraction between each other and are the cause of an additional secondary source of contraction. Only for the weakest interactions, the linear behavior does not hold. The reason lies of course in the presence of the lateral deviations. They can be characterized by measuring $R_{g,r}(n)$

$$R^2_{g,r}(n) = \frac{1}{n}\sum_{i=1}^{n}\left[\left(r^i_x - r^0_x\right)^2 + \left(r^i_y - r^0_y\right)^2\right]. \qquad (8)$$

This is essentially the radius of gyration of the magnetic beads in the plane perpendicular to the external field or dipole directions.

The results of the width of the chains are shown in fig. 6(b). With increasing length, the width of the dipolar chains grows but remains, with values less than σ, fairly small. On increasing the interaction strength the lateral spread of beads is diminished, which is indicated by the corresponding decrease in slope of the various curves. Similar to the end-to-end distance, also here the interaction between more distant magnetic beads within a dipolar chain causes an additional effect indicated by the concave behavior of the curves. Here, however, it results in a increased suppression of the lateral movement of nano-particles within longer chains at the same interaction strength.

It should be noted that the estimated errors in fig. 6 for some of the points is relatively large. This mainly occurs at the large n value for the various curves and is caused by the fact that only a few chains of the corresponding size were observed within the simulation time. Accordingly, the measurements include contributions from the merging process and unstable chains and therefore these larger fluctuations are to be expected.

6 Density profiles

The formation of dipolar chains has a significant impact on the internal structure of the star-polymers. In particular, the isotropy of non-functionalized star-polymers, which is still recovered for weak interaction strengths λ, is broken. We can examine this feature more closely by considering the density profiles of the magnetic beads with respect to the center of mass of the full star-polymer. Here we can in a natural fashion distinguish two types of density profiles. The first is $\rho_r(r)$ and is measured in the direction perpendicular to the external magnetic field. The second type of density profile, $\rho_z(z)$, is measured along the field direction. Results of these measurements are presented in figs. 7 and 8, which complement each other by showing selected

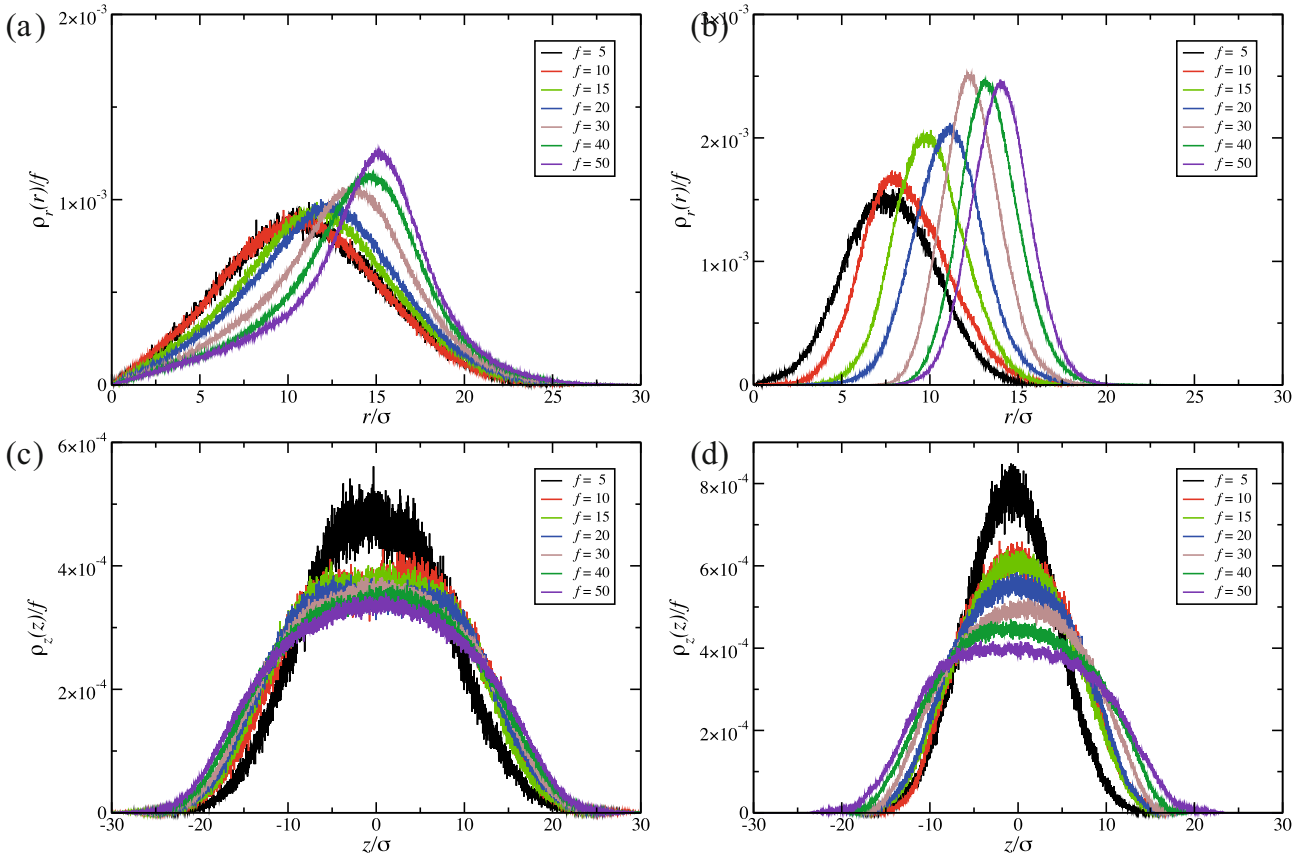

Fig. 8. The density profiles (a), (b) $\rho_r(r)/f$ and (c), (d) $\rho_z(z)/f$ of magnetic particles with respect to the center of mass of the star-polymer, for interaction strength (a), (c) $\lambda = 40$ and (b), (d) $\lambda = 100$ and for various functionalities f (as labeled).

density profiles for fixed functionality and constant interaction strength, respectively. To facilitate the comparison, we plot the density profiles normalized with the functionality, *i.e.*, the probability distribution functions.

In fig. 7, where we display the density profiles for the functionality $f = 10$ and $f = 50$, we note that for weak interaction strengths $\lambda \lesssim 50$ the 2D-radial density profiles $\rho_r(r)$ show an initially linear behavior for small r-values. This is even more clearly visible in fig. 8(a), and is a consequence of measuring a 2D-profile for what is an almost spherical symmetric 3D-density distribution. More interesting, however, is the fact that on augmenting the interaction strength the initial wide distributions change into rather narrow profiles peaked at a well-defined distance from the center of the star that does not depend on the interaction strength. This observation can be attributed to the narrow lateral distribution of magnetic beads within the chains, as we demonstrated in fig. 6(b). The collective distance of beads is, with respect to the weak interaction limit, drawn to the center of the star-polymer by the pulling of arms that connect to the outer ends of the chain, but is at the same time repelled by the steric interaction near the center and the entropic loss of the polymer arms.

The other set of profiles, $\rho_z(z)$, shows that the formation of the chains draws the beads toward the equatorial plane. Also here the arms that connect to the outer ends of the chain play an important role, but now the pulling force is due to the imbalance of the forces along the field direction between different ends of the chain. The strength of this confining force depends on the length of the dipolar chains that are formed and therefore increases with increasing magnetic interaction parameter λ. The resulting distributions get narrower, but even for the largest interaction strength in the case $f = 10$ the width is about 50% larger than the length of the chains. In the case of the higher functionality $f = 50$ we even get distributions that display a plateau, which is caused by a combination of longer and more chains with respect to the functionality $f = 10$. The fact that the plateaus are not completely flat, can be understood by realizing that among the simulations at identical conditions not all chains are equally long and the shorter chains are more mobile.

The density distributions shown in fig. 8 for fixed interaction strengths $\lambda = 40$ and $\lambda = 100$, that correspond to a moderate and strong interaction, respectively, reveal the effect that functionality has on the location of the dipolar chains. The positions of the chains for higher functionalities are pushed outwards due to the increase in steric interactions arising in the vicinity of the core in a natural fashion, and to a lesser extent by the increase in average chain length. The latter is also responsible for the broadening of the $\rho_z(z)$ profiles.

7 Conclusion

We have examined the conformational behavior of single isolated star-polymers with functionalized end-groups. In particular end-groups formed by super-paramagnetic nano-particles, whose magnetic interaction strength can be controlled directly by the application of an external magnetic field. To this end we formulated a basic simulation model that enables us to explore, in a semi-qualitative fashion, the main features of conformations that such macromolecules have if they would be synthesized.

Within this model, we assume that the external magnetic field induces dipoles in the nano-particles that are, at all time, perfectly aligned along the field direction. Consequently, the nano-particles form on increasing the field strength, dipolar chains in the same direction. Whereas the length of such chains for free dipolar particles could grow to arbitrary length, here their number is limited by the functionality of the star-polymer. Moreover, the chain length is also restricted by their connectivity to the core of the star-polymer by a finite polymer string. The main features of the resulting single-star configuration diagram in the plane of functionality and interaction strength show that i) an increasing number of dipolar chains is formed for higher star-functionality, and ii) an increase in their length on augmenting the magnetic interaction strength can be observed. This is qualitatively similar to the single-star self-assembly behavior found for telechelic star-polymers [18,19], where the driving force is due to the differences in solubility of the head and tails of the polymer chains. In both systems, the aggregation process creates a patchy-like structure; however, while for the telechelic stars the patches are compact and roughly spherical in nature, we find here elongated "patches". Moreover, the telechelic stars can freely rotate in the solvent, whereas the orientation of magnetically functionalized star-polymers is enslaved by the direction of the external magnetic field.

The formation of chains also results in a more compact star for increasing interaction strengths. Especially for low functionality its overall size and shape is significantly affected. This is caused by the preference of forming longer dipolar chains, which for low functionality star-polymers will be only one. Consequently the center of mass of the star and the anchor point of the polymer arms separate, resulting in a watermelon structure and correspondingly in an aspherical shape. For higher functionalities, the overall shape of the polymer-star remains spherical, while embedding several longer chains.

The relative importance of entropic and magnetic interactions, separates a weak field region, with many small chains that can easily break up, from the strong interaction region with fewer and longer chains, that are much more stable over time. Consequently, the probability distribution of the length of dipolar chains changes from an exponential behavior to a unimodal distribution with a preferred averaged chain length. The individual chains, however, are for all interaction strengths very straight and narrowly confined in the direction perpendicular to the external field. The lateral movement of the full chain is, due to the architecture of the macromolecules, confined to a few particle diameters. Although there is a preferential position near the equatorial plane for the aggregated chains, they are only weakly confined along the field direction.

The qualitative picture that arises from our simulations is clear, even though some aspects of the magnetic interaction were simplified. We discarded inhomogeneities in the magnetic particles and the perfect alignment with the external field is only true in a first approximation, because the induced magnetic dipoles affect each other locally as well. A more interesting question, however, is the effect of our choice of super-paramagnetic nano-particles on the behavior of the star-polymer. A different choice would have been to consider permanent magnetic particles. In such a system, the magnetic chains that would be formed will be more flexible and can close up to form rings. In addition, the number of magnetic units that would participate in such chains is less restricted by the finite polymer strain connecting them to the core of the star-polymer.

For telechelic star-polymers it was shown that the properties that were found for the isolated macromolecules persisted also when going to finite densities; further their patchiness could be used to stabilize various crystals by tuning functionality and interaction strength. Whether similar features can also be identified for these magnetically functionalized star-polymers is not obvious and is postponed, in combination with the development of a suitable coarse-graining strategy for these molecules, for future research.

Open access funding provided by University of Vienna. This work was financially supported by the Austrian Science Fund FWF within the SFB ViCoM (F41) and computing time provided by the Vienna Scientific Cluster is gratefully acknowledged. We thank Gerhard Kahl for a careful reading of the manuscript and helpful discussions.

Author contribution statement

Ronald Blaak performed the simulations and analysis. Christos N. Likos suggested the problem and co-designed the research.

References

1. A.K. Khandpur, S. Foerster, F.S. Bates, I.W. Hamley, A.J. Ryan, W. Bras, K. Almdal, K. Mortensen, Macromolecules **28**, 8796 (1995).
2. N.P. Balsara, M. Tirrell, T.P. Lodge, Macromolecules **24**, 1975 (1991).
3. C.L. Elkins, K. Viswanathan, T.E. Long, Macromolecules **39**, 3132 (2006).
4. J. Chen, N. Seeman, Nature **350**, 631 (1991).

5. E. Andersen, M. Dong, M. Nielsen, K. Jahn, R. Subramani, W. Mamdouh, M.M. Golas, B. Sander, H. Stark, C.L.P. Oliveira, J. Pedersen, V. Birkedal, F. Besenbacher, K.V. Gothelf, J. Kjems, Nature **459**, 73 (2009).
6. P.W.K. Rothmund, Nature **440**, 297 (2006).
7. R.G. Winkler, D.A. Fedosov, G. Gompper, Curr. Opin. Colloid Interface Sci. **19**, 594 (2014).
8. D. Vlassopoulos, M. Cloitre, Curr. Opin. Colloid Interface Sci. **19**, 561 (2014).
9. C. Micheletti, D. Marenduzzo, E. Orlandini, Phys. Rep. **504**, 1 (2011).
10. M. Ballauff, C.N. Likos, Angew. Chem. Int. Ed. **116**, 3060 (2004).
11. C.N. Likos, Soft Matter **2**, 478 (2006).
12. M. Pitsikalis, N. Hadjichristidis, J.W. Mays, Macromolecules **29**, 179 (1996).
13. D. Vlassopoulos, T. Pakula, G. Fytas, M. Pitsikalis, N. Hadjichristidis, J. Chem. Phys. **111**, 1760 (1999).
14. F. Lo Verso, A.Z. Panagiotopoulos, C.N. Likos, Phys. Rev. E **79**, 010401 (2009).
15. C. Koch, C.N. Likos, A.Z. Panagiotopoulos, F.L. Verso, Mol. Phys. **109**, 3049 (2011).
16. F. Lo Verso, C.N. Likos, C. Mayer, H. Löwen, Phys. Rev. Lett. **96**, 187802 (2006).
17. F. Lo Verso, C.N. Likos, H. Löwen, J. Phys. Chem. C **111**, 15803 (2007).
18. B. Capone, I. Coluzza, F.L. Verso, C.N. Likos, R. Blaak, Phys. Rev. Lett. **109**, 238301 (2012).
19. B. Capone, I. Coluzza, R. Blaak, F.L. Verso, C.N. Likos, New J. Phys. **15**, 095002 (2013).
20. I. Nezbeda, J. Kolafa, Y.V. Kalyuzhnyi, Mol. Phys. **68**, 143 (1989).
21. M.H. Ford, S.M. Auerbach, P.A. Monson, J. Chem. Phys. **121**, 8415 (2004).
22. A. Lomakin, N. Asherie, G.B. Benedek, Proc. Natl. Acad. Sci. U.S.A. **96**, 9465 (1999).
23. G.M. Whitesides, M. Boncheva, Proc. Natl. Acad. Sci. U.S.A. **99**, 4769 (2002).
24. A.B. Pawar, I. Kretzschmar, Macromol. Rapid Commun. **31**, 150 (2010).
25. E. Bianchi, R. Blaak, C.N. Likos, Phys. Chem. Chem. Phys. **13**, 6397 (2011).
26. L. Rovigatti, B. Capone, C.N. Likos, Nanoscale **8**, 3288 (2016).
27. C.W. Jung, P. Jacobs, Magn. Reson. Imaging **13**, 661 (1995).
28. H. Wang, Y. Yu, Y. Sun, Q. Chen, Nano **06**, 1 (2011).
29. J.D. Weeks, D. Chandler, H.C. Andersen, J. Chem. Phys. **54**, 5237 (1971).
30. G.S. Grest, K. Kremer, T.A. Witten, Macromolecules **20**, 1376 (1987).
31. A. Arnold, O. Lenz, S. Kesselheim, R. Weeber, F. Fahrenberger, D. Roehm, P. Košovan, C. Holm, in *Meshfree Methods for Partial Differential Equations VI*, Lect. Notes Comput. Sci. Eng., Vol. **89** (Springer, Berlin, Heidelberg, 2013) pp. 1–23.
32. S. Huissmann, R. Blaak, C.N. Likos, Macromolecules **42**, 2806 (2009).
33. K. Šolc, J. Chem. Phys. **55**, 335 (1971).